PAPER

Check for updates

CO$_2$ hydrogenation to formic acid on Pd–Cu nanoclusters: a DFT study†

D. Chattaraj [ID] *[a] and C. Majumder[b]

Carbon dioxide (CO$_2$) hydrogenation to formic acid is a promising method for the conversion of CO$_2$ to useful organic products. The interaction of CO$_2$ with hydrogen (H$_2$) on Pd$_m$Cu$_n$ ($m + n$ = 4, 8 and 13) clusters to form formic acid (HCOOH) has been explored using density functional theoretical (DFT) calculations. Pd$_2$Cu$_2$, Pd$_4$Cu$_4$ and 13-atom Pd$_{12}$Cu clusters are found to be the most stable among all of the Pd$_m$Cu$_n$ ($m + n$ = 4, 8 and 13) clusters with binding energies of -1.75, -2.16 and -2.40 eV per atom, respectively. CO$_2$ molecules get adsorbed on the Pd$_2$Cu$_2$, Pd$_4$Cu$_4$ and Pd$_{12}$Cu clusters in an inverted V-shaped way with adsorption energies of -0.91, -0.96 and -0.44 eV, respectively. The hydrogenation of CO$_2$ to form formate goes through a unidentate structure that rapidly transforms into the bidentate structure. To determine the transition state structures and minimum energy paths (MEPs) for CO$_2$ hydrogenation to formic acid, the climbing image nudge elastic band (CI-NEB) method has been adopted. The activation barriers for the formation of formic acid from formate on Pd$_2$Cu$_2$ and Pd$_4$Cu$_4$ are calculated to be 0.79 and 0.68 eV, respectively whereas that on the Pd$_{12}$Cu cluster is 1.77 eV. The enthalpy for the overall process of CO$_2$ hydrogenation to formic acid on the Pd$_2$Cu$_2$, Pd$_4$Cu$_4$ and Pd$_{12}$Cu clusters are found to be 0.83, 0.48 and 0.63 eV, respectively. Analysis of the density of states (DOS) spectra show that the 4d orbital of Pd, the 3d orbital of Cu, and the 2p orbitals of C and O atoms are involved in the bonding between CO$_2$ molecules and the Pd$_2$Cu$_2$ clusters. The CO$_2$ adsorption on the Pd$_m$Cu$_n$ ($m + n$ = 4 and 8) clusters has also been explained in terms of the charge density distribution analysis.

Introduction

In recent decades, increased consumption of fossil fuels has resulted in a significant increase in the concentration level of carbon-dioxide (CO$_2$) in the atmosphere. This has changed the global climate and caused ocean acidification.[1–4] CO$_2$ sequestration, carbon capture and storage have been suggested as different new ways to manage global CO$_2$ levels. However, the

[a] Product Development Division, Bhabha Atomic Research Centre, Trombay, Mumbai 400085, India. E-mail: debchem@barc.gov.in; Fax: +91 22 2550 5151; Tel: +91 22 2559 6446

[b] Chemistry Division, Bhabha Atomic Research Centre, Trombay, Mumbai 400085, India

† Electronic supplementary information (ESI) available: See supplementary Tables S1 and S2 (ESI†) for binding energies and bond lengths of different adsorbates adsorbed on Pd$_4$Cu$_4$ and Pd$_{12}$Cu clusters, respectively; Tables S3–S5 for the different geometric isomers of Pd$_m$Cu$_n$ ($m + n$ = 4, 8 and 13) clusters and Tables S6–S8 for the charge density distribution of Pd$_m$Cu$_n$ ($m + n$ = 4, 8 and 13) clusters. See supplementary Fig. S1 and S2 for the lowest energy structure of Pd$_4$Cu$_4$ and Pd$_{12}$Cu clusters along with different adsorbates on those clusters, respectively; S3 and S4 for the potential energy profile of CO$_2$ hydrogenation to formic acid on Pd$_4$Cu$_4$ and Pd$_{12}$Cu clusters, respectively; S5 and S6 for the density of states of Pd$_4$Cu$_4$ and Pd$_{12}$Cu clusters along with their CO$_2$ adsorbed counterparts, respectively. See DOI: **https://doi.org/10.1039/d2cp03805f**

catalytic conversion of CO$_2$ into useful chemical products *e.g.* methane (CH$_4$), methanol (CH$_3$OH) and formic acid (HCOOH) has attracted considerable attention in recent years.[5–14] CO$_2$ is abundant in nature; it is an inexpensive feed stock for chemical processes and its removal from the atmosphere will reduce the greenhouse effect significantly. One very good example is CO$_2$ conversion to the useful liquid hydrocarbon formic acid (HCOOH) through hydrogenation. Formic acid is an important chemical used in making animal feed, in tannery and dying leather and textiles and as a food preservative.[15] Currently, formic acid synthesis is mainly performed through a two-step process: (i) carbonylation of methanol to methyl formate (HCOOCH$_3$) using a high pressure of toxic CO as the feedstock and (2) hydrolysis of HCOOCH$_3$ to formic acid and methanol. Formic acid production by direct hydrogenation of CO$_2$ is a promising alternative way in terms of economy, ecology and safety. CO$_2$ is extremely stable both thermodynamically and kinetically, exhibiting negative reaction entropies and high Gibb's energies. Hence, an effective, cheap and recyclable catalyst for this conversion of CO$_2$ to formic acid and methanol is urgently required.

A number of reports on experimental and theoretical studies of CO$_2$ conversion to methanol and formic acid catalytically on

metallic and bimetallic surfaces have been reported.[16,17] Several Cu based catalysts like Pd–Cu, Ga–Cu, Ni–Cu, Co–Cu, Cu/ZnO and Cu/ZrO have been developed experimentally for enhancing the conversion of CO_2 to CH_3OH and $HCOOH$.[18–21] Among these, a Pd–Cu catalyst is one of the most active bimetallic catalysts for CO_2 hydrogenation. Pd has been widely used as a promising catalyst to enhance CO/CO_2 hydrogenation. Melian-Cabrera et al. have found that the reduced state of Cu has been maintained via hydrogen spill over by Pd doped Cu-based catalysts.[22] The reducibility of Cu sites is enhanced by Pd addition because of electron donation from Pd. The Pd–Cu catalysts exhibit a strong synergistic promotion of the methanol formation rate compared to that of pure Cu because of the combination of Cu and Pd. In the DFT study by Liu et al., a Cu(111) surface with a Pd monolayer substituted on the top-most layer has been employed as a Pd–Cu bimetallic system to explore the underlying mechanism of methanol synthesis from CO_2 hydrogenation.[19] In formic acid formation, CO_2 hydrogenation is one of the most important steps. In this aspect, it is assumed that bimetallic Pd–Cu can act as a good catalyst for formic acid formation also. The experimental studies are not sufficient to elucidate a catalytic process over the catalytic surface and therefore, DFT calculations are essential to illustrate the reaction mechanism of CO_2 hydrogenation on bifunctional catalyst.

A large number of transition metal complexes, mostly Ir, Rh and Ru-based ones, have been used for CO_2 hydrogenation to formic acid. In recent times, the synthesis of formates and formic acid using homogeneous catalysis have been reviewed by several research groups.[16,17,23–25] Sredojevic et al. have studied the formic acid synthesis by CO_2 hydrogenation over single-atom catalysts based on Ru and Cu embedded in graphene.[26] They made this synthesis possible with low activation energy by proceeding with the mechanism of H_2 dissociation over the metal atom prior to CO_2 adsorption. A Ni and Ni–Fe bimetallic system has also been found to be suitable for CO_2 reduction to formic acid and other valuable chemicals.[27,28] Most recently, Liu et al. have reported CO_2 hydrogenation to formate and formic acid by a bimetallic palladium-copper hydride cluster.[29] The reaction between $PdCuH_4^-$ and CO_2 to produce formic acid and $PdCuH_2^-$ has been analysed by mass spectrometric analysis. Different isomers of $PdCuH_4^-$ and $PdCuCO_2H_4^-$ are identified by anion photo electron spectroscopy (PES) and electronic structure calculations. Their mechanistic study confirms the metastable structure as the catalytic driving force.

Hydrogen adsorption, dissociation and diffusion on the PdCu surface has been shown in our earlier study.[30] If CO_2 gets adsorbed on the PdCu surface, the CO_2 reduction to formic acid and methanol is possible. Aiming for this, using DFT, we have investigated CO_2 adsorption on the PdCu surface with all possible orientations. But, it has been found that the PdCu surface does not adsorb CO_2 in ambient conditions. In our next attempt, we have partially substituted the Pd atoms with Pt, and the Cu atoms with Ag, and Au on the PdCu surface to see whether the CO_2 molecule gets adsorbed or not. It is observed that the CO_2 molecule does not get adsorbed in any of these compositions of the PdCu surface. As, CO_2 does not get adsorbed on the PdCu surface, the target of CO_2 reduction to formic acid has been eliminated. Further, we have focused on the finite size of the PdCu clusters which have a large surface area, a high number of dangling bonds and large number of active sites. CO_2 adsorption on the Pd_mCu_n ($m + n$ = 4, 8 and 13) clusters has been studied using DFT based computational methodology. It is found that CO_2 gets adsorbed on the Pd_mCu_n ($m + n$ = 4, 8 and 13) clusters. As, the PdCu clusters also take a H_2 molecule, the CO_2 reduction to formic acid has been studied here on the Pd_mCu_n ($m + n$ = 4, 8 and 13) clusters.

Although many researchers have focussed on CO_2 hydrogenation for formic acid and methanol synthesis, to the best of our knowledge, formic acid formation from CO_2 on nanoclusters, especially, Pd–Cu nanoclusters is rare. Nanoparticles have a high surface to volume ratio and better reactivity compared to their surface and bulk counterparts, so they can act as a better catalyst compared with those forms. Any real-life catalytic system would require the use of a support system. Here, small PdCu clusters are considered to study the basic reaction mechanism of formic acid formation by CO_2 hydrogenation. By considering reactions on free clusters, which have higher degrees of freedom, it is possible to underscore the reaction mechanism at the smallest scale length. The results of these calculations are useful to study the reaction mechanism on supported clusters. Here, in this computational study, formic acid formation by CO_2 hydrogenation on Pd–Cu nanoclusters has been investigated using a DFT formalism.

The geometry, energetics and reaction mechanism are of prime importance for the synthesis of formic acid on the bimetallic clusters. Here, CO_2 hydrogenation with H adsorbed on the Pd_mCu_n ($m + n$ = 4, 8 and 13) clusters is systematically studied using a state of the art first principles method for the generation of formic acid. The reaction pathways for the conversion of CO_2 to formic acid have been revealed by a nudge elastic band (NEB) method. The calculated properties for the formic acid formation provide comprehensive data which will be useful for experimental understanding.

Results and discussion

Structural optimization of Pd_mCu_n ($m + n$ = 2, 4, 8 and 13) clusters

Dimer ($m + n$ = 2). The binding energy, bond length and spin moment of the PdCu dimer along with its constituent element dimers Pd_2 and Cu_2 have been calculated with and without a spin–orbit coupling scheme and are given in Table 1.[31–34] From Table 1, it is found that the spin–orbit coupling effect has no significant contribution in the binding energies and bond lengths of the clusters. Hence, the entire calculation has been performed without including the spin–orbit coupling effect. The above mentioned properties of the dimers are calculated to test the accuracy of the theoretical method employed for the total energy calculation and the reliability of the potential used

Table 1 Calculated and experimental binding energies and bond lengths of the Pd_2, Cu_2 and PdCu dimers

Cluster (s)	Binding energy (eV per atom)			Bond length (Å)		
	Calc. (NSO)	Calc. (SO)	Expt	Calc. (NSO)	Calc. (SO)	Expt
Pd_2	−0.64	−0.65	−0.51[43]	2.48	2.49	2.48[44]
Cu_2	−1.12	−1.12	−1.04[45]	2.22	2.22	2.21[46]
PdCu	−0.91	−0.92	—	2.32	2.33	—

NSO = non spin–orbit, SO = spin–orbit.

Table 2 Average binding energy (B.E), average bond length (Pd–Cu) and spin moments of the Pd_mCu_n ($m + n$ = 4, 8 and 13) clusters

Number of atom (n)	System	Average B.E. (eV per atom)	Average Pd–Cu B.L. (Å)	Spin moment (μ_B)
$n = 4$	Pd_4	−1.67	2.60 (Pd–Pd)	0
	Pd_3Cu	−1.74	2.50	1
	Pd_2Cu_2	−1.75	2.47	0
	$PdCu_3$	−1.62	2.46	1
	Cu_4	−1.59	2.25 (Cu–Cu)	0
$n = 8$	Pd_8	−2.07	2.67 (Pd–Pd)	2
	Pd_7Cu	−2.10	2.54	3
	Pd_6Cu_2	−2.09	2.51	2
	Pd_5Cu_3	−2.15	2.50	1
	Pd_4Cu_4	−2.16	2.56	0
	Pd_3Cu_5	−2.09	2.50	1
	Pd_2Cu_6	−2.14	2.55	2
	$PdCu_7$	−2.13	2.56	1
	Cu_8	−2.14	2.28 (Cu–Cu)	0
$n = 13$	Pd_{13}	−2.32	2.73 (Pd–Pd)	8
	$Pd_{12}Cu$	−2.40	2.60	7
	$PdCu_{12}$	−2.28	2.62	4
	Cu_{13}	−2.24	2.53 (Cu–Cu)	5

here. The calculated values with PBE are given in Table 1 and are compared with the reported experimental values. The calculated bond length and binding energy heteroatomic PdCu dimer is found to be comparable with other reported theoretical data.[35]

After establishing the properties of the PdCu dimer, the total energy and binding energy of different Pd_mCu_n ($m + n$ = 4, 8 and 13) clusters are calculated. A large number of geometrical isomers of each composition of the Pd_mCu_n ($m + n$ = 4, 8 and 13) clusters are shown in Tables S3–S5 (ESI†). The specific coordinates of the clusters are given in Table S9 (ESI†). The results reveal that the small PdCu clusters favor a 1 : 1 composition (*e.g.* Pd_2Cu_2, Pd_4Cu_4) and for the 13-atom cluster it is $Pd_{12}Cu$ where the Cu atom is at the centre of the icosahedron. The ground state geometric configurations for each composition of the Pd_mCu_n ($m + n$ = 2, 4, 8 and 13) clusters are shown in Fig. 1.

Tetramer ($m + n$ = 4). The tetramer is an important model for investigating several catalytic processes.[36–40] The structure of the tetramer also plays a significant role in cluster growth as this is the smallest size where clusters can possess either a planar or non-planar geometry. This provides an initial clue for understanding the structural pattern of larger size clusters *i.e*, pentamer onward. For tetramer ($m + n$ = 4) heteroatomic clusters, three compositions (1 : 3, 2 : 2 and 3 : 1), apart from the homoatomic clusters, are considered for calculation. Accordingly, the various possible isomeric structures of Pd_4, Cu_4, Pd_3Cu, Pd_2Cu_2 and $PdCu_3$ clusters are optimized. The average binding energy, average bond length and spin moments of these clusters are summarized in Table 2.

The binding energies of the Pd_mCu_n clusters are shown in Table 2. It is seen that Pd_2Cu_2 is the most stable structure among all of the Pd_mCu_n ($m + n$ = 4) clusters with the average binding energy of −1.75 eV per atom. Table S3 (ESI†) shows that Pd_4 forms a triangular pyramid (Tpy) structure as the

lowest energy with an average Pd–Pd bond length of 2.60 Å. The substitution of a single Pd atom by a Cu atom in Pd_4 resulting in Pd_3Cu does not change the Tpy geometry and the average Pd–Cu bond length for that is found to be 2.50 Å. Further substitution of a Pd atom in Pd_3Cu forming Pd_2Cu_2 does not allow a change of its Tpy geometry and here the average Pd–Cu bond length is found to be 2.47 Å. The further substitutions of the Pd atoms in Pd_2Cu_2 resulting in $PdCu_3$ and Cu_4 changes the geometry to planar rhombus. The Pd_2Cu_2 cluster can be visualized as a combination of a maximum of two PdCu dimer moieties which gives stability to Pd_2Cu_2 whereas in Pd_3Cu and $PdCu_3$ only one PdCu dimer moiety is present. The spin moment of both Pd_4 and Cu_4 clusters are calculated to be 0 μ_B. The substitution of Pd atoms in the Pd_4 cluster and Cu atoms in the Cu_4 cluster increases the spin moment except for Pd_2Cu_2 which is paramagnetic in nature.

Octamer ($m + n$ = 8). The atomic and electronic structure of Pd_mCu_n ($m + n$ = 8) has been investigated through all composition ranges. We have considered several initial structures and those have been optimized to find out the most stable one among them. Based on the comparison of the relative energies, the homoatomic Pd_8 and Cu_8 clusters are found to favour bicapped octahedron structures as shown in Table S4 (ESI†). The average bond length of Pd–Pd and Cu–Cu are 2.67 Å and 2.28 Å, respectively. The geometry of other low-lying isomers,
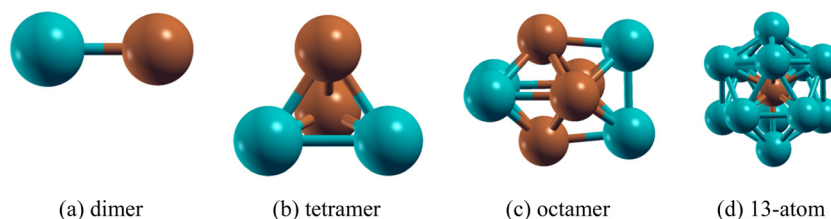
Fig. 1 Stable isomers of the Pd_mCu_n ($m + n$ = 2, 4, 8 and 13) clusters (a) dimer (b) tetramer (c) octamer (d) 13-atom cluster (atomic colours: green = Pd, brown = Cu).

(a) dimer   (b) tetramer   (c) octamer   (d) 13-atom

close to the lowest energy isomer, along with the bond length and spin moment are listed in Table S4 (ESI†). In alloy clusters, the equiatomic Pd_4Cu_4 moiety also forms a bicapped octahedron geometry, like Pd_8 and Cu_8, with a particular type of arrangement of the Pd and Cu atoms as shown in Fig. 1. All of the possible isomers of Pd_4Cu_4 are shown in Table S4 (ESI†) along with corresponding energy values. There are two close energy isomers of Pd_4Cu_4. In the most stable one, the two capped positions outside the main octahedron unit are constituted by two Pd atoms and an edge of the octahedron is also made up by two Pd atoms. The remaining atoms of the bicapped octahedron or dodecahedron are four Cu atoms. The close energy structure of the dodecahedron Pd_4Cu_4 moiety is a Cu-capped pentagonal bi-pyramid. The difference in energy between these two structures is 0.16 eV.

13 Atom cluster ($m + n = 13$). The 13 atom cluster, also called a magic cluster, has a unique identity as it bears interesting properties because of its higher relative structural and energetic stability.[41–44] It generally possesses an icosahedron structure with the central atom having the coordination number 12. This coordination resembles the FCC bulk structure. Thus, it is obvious; the difference between a 13 atom cluster and the bulk is mainly due to size and shape effects. This present study is focused on formic acid formation by CO_2 hydrogenation on different size PdCu clusters including a 13 atom moiety. As a requirement, the most stable structure of $PdCu_{12}$ and $Pd_{12}Cu$

has been established along with the icosahedron Pd_{13} and Cu_{13} clusters. In order to obtain the lowest energy isomer of the $Pd_{12}Cu$ cluster, one Pd atom was replaced by Cu at different positions of the Pd_{13} icosahedron *i.e.*, Cu at the apex and Cu at the centre. On the basis of the total energy considerations, the icosahedron with the Cu atom at the centre position forms the lowest energy isomer of the $Pd_{12}Cu$ cluster (see Fig. 1(d)). The close energy structures of $Pd_{12}Cu$ are given in Table S5 (ESI†). The binding energy and average bond lengths (Pd–Cu and Pd–Pd) are shown in Table 2. The total spin moment of this cluster is 7.0 μ_B. But, the $PdCu_{12}$ icosahedron with the Pd atom at the apex position forms the lowest energy isomer of that cluster. The total spin moment of that $PdCu_{12}$ cluster is calculated to be 4.0 μ_B.

Formic acid formation on Pd_mCu_n ($m + n$ = 4, 8 and 13) clusters

CO_2 hydrogenation to formic acid on Pd_2Cu_2 tetramer. First, the adsorption behaviour of H_2 molecules on the Pd_2Cu_2 cluster has been studied (see Fig. 2). For optimization, the H_2 molecule is placed on top of the Pd as well as the Cu atoms. The distance of the H atoms from the Pd/Cu atoms is kept 3 Å and the H–H bond length as 0.75 Å. The results show that the H attached to the top of Pd forms the lowest energy isomer as shown in Fig. 2(a). The energy released during the H_2 adsorption on Pd is estimated to be −5.05 eV. After optimization, the Pd–H and H–H bond lengths become 1.75 Å and 0.86 Å,
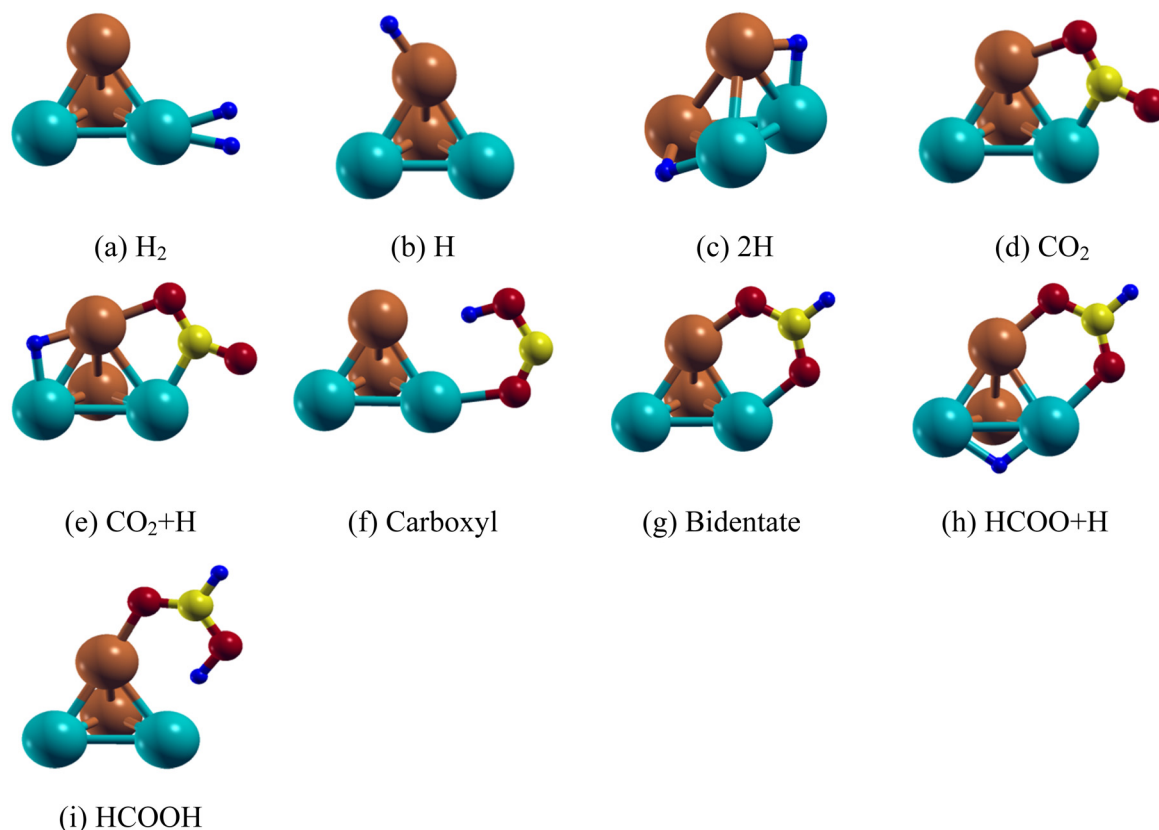

Fig. 2 Lowest energy structure of the Pd_2Cu_2 clusters along with their (a) H_2 (b) H (c) 2H (d) CO_2 (e) CO_2 + H (f) carboxyl (g) bidentate (h) HCOO + H and (i) HCOOH adsorbed species.

This journal is © the Owner Societies 2023

Phys. Chem. Chem. Phys., 2023, **25**, 2584–2594 | **2587**

respectively. The increase in the H–H bond length from equilibrium separation suggests activation of the bond. Other than molecular adsorption, the adsorption of the H-atom on the top, bridge and hollow sites of Pd_2Cu_2 cluster is also investigated. The results show that the H atom favours the on-top Cu location as shown in Fig. 2(b). The energy released is found to be −2.05 eV and the average Cu–H distance is 1.51 Å. The stability of two H atoms on the Pd_2Cu_2 cluster has also been investigated. It is found that both the H atoms prefer to bind with the Cu–Pd bridge sites as shown in Fig. 2(c). The binding energy for these two H atoms is calculated to be −5.19 eV with Cu–H and Pd–H bond lengths of 1.75 and 1.80 Å, respectively.

We have first studied the CO_2 adsorption on the Pd_2Cu_2 cluster which is the primary step for HCOOH formation. The most stable configuration of CO_2 on the Pd_2Cu_2 shows that one of the C–O bonds is attached in such a way so that C and O atoms are attached to the Pd and Cu atoms, respectively as shown in Fig. 2(d). The binding energy of CO_2 is −0.91 eV. The optimum lengths of the Cu–O and Pd–C bonds are 2.00 and 1.99 Å, respectively. As a consequence, the C–O bond is elongated from 1.16 Å (free CO_2) to 1.26 Å. The O–C–O bond angle of the adsorbed CO_2 is optimized to 139.8°. Another possibility of CO_2 adsorption on the Pd_2Cu_2 cluster could be where the C and O atoms could be attached to the Cu and Pd atoms. However, this configuration is unstable. The reason behind this is the extent of electron transfer between Cu–O and Pd–C in the CO_2 adsorbed Pd_2Cu_2 cluster. The details have been discussed in DOS analysis in the Electronic structure section.

On the basis of previous literature, it is seen that formic acid formation by hydrogenation of CO_2 can take place either through formate (HCOO•) or carboxyl (COOH) radical formation. For the Pd_2Cu_2 cluster, the formate route is found to be more favorable than the carboxyl route. This fact is also established here by calculating the activation energy of the corresponding processes which are discussed in later sections. Two configurations are possible for the HCOO species, carboxyl (mono-HOCO) and bidentate (bi-HCOO), distinguished by the number of O atoms that are adsorbed on the Pd_2Cu_2 cluster. For carboxyl, one of the two O atoms of HOCO gets attached to the Pd atom of the Pd_2Cu_2 cluster, respectively as shown in Fig. 2(f). The Pd–O and Cu–H bond distances are found to be 1.14 Å and 2.33 Å, respectively. The adsorption energy for carboxyl (mono-HOCO) is found to be −1.21 eV. Another possibility of carboxyl radical (mono-HOCO) adsorption on Pd_2Cu_2 happens where the O and H atoms of HOCO are

attached to Cu and Pd atoms, respectively. However, this route is found to be not stable.

For bidentate-complex ($HCOO$-Pd_2Cu_2) formation, two O atoms are connected to the Pd–Cu edge of the Pd_2Cu_2 cluster as shown in Fig. 2(g) with an adsorption energy of −3.39 eV. The optimized Pd–O and Cu–O bond lengths are 2.14 and 1.94 Å, respectively. The O–C–O bond angle is 128.6° and the C–H bond length is 1.10 Å for the HCOO adsorbed on the Pd_2Cu_2 cluster. In this context it should be noted that here CO_2 gets adsorbed on the Pd_2Cu_2 cluster in a V-shaped orientation, but addition of an H atom to the C of CO_2 makes it possible to adsorb bidentate HCOO in an inverted V-fashion. This is because of depletion of electronic charge on the O atom which gets attached to the Pd and Cu atoms. The DOS analysis in the Electronic structure section supports this statement.

The final step is formic acid formation from bidentate formate by adding an H-atom. The adsorption of formic acid on the Pd_2Cu_2 cluster has two possibilities; the H atom is either attached to a Cu or a Pd atom of the cluster. It is seen that the H atom of the COOH attached to a Pd atom of Pd_2Cu_2 has relatively lower energy compared to that of the H attached to a Cu atom. The Pd–H configuration (Fig. 2(i)) is found to be 0.29 eV lower in energy than Cu–H configuration. The adsorption energy of the Pd–H configuration is calculated to be −1.37 eV. The Pd–H and Cu–O distances in the lower configuration are 1.96 Å and 1.95 Å, respectively. The binding energies and related bond lengths of H_2, H, 2H, CO_2, HCOO and HCOOH adsorbed on the Pd_2Cu_2 nanocluster are given in Table 3.

The reaction between H and CO_2 on Pd_mCu_n ($m + n = 4, 8$ and 13) leads to the formation of bidentate formate whereas that between H and formate forms formic acid. For that, co-adsorption of H and CO_2 as well as H and formate HCOO on the Pd_mCu_n ($m + n = 4, 8$ and 13) clusters has been investigated. In the first case, H has been placed in different adsorption sites (top, bridge and hollow) of the model cluster keeping CO_2 adsorbed at a fixed site. The results show that H on the Pd–Cu edge opposite to the CO_2 adsorbed edge has the most stable geometry as shown in Fig. 2(e). The H adsorption energy in the pre-adsorbed Pd_2Cu_2–CO_2 cluster is −2.36 eV as per eqn (7). On the other hand, H is found to be stable on the Pd–Pd edge of the pre-adsorbed bidentate formate (Pd_2Cu_2–HCOO) complex (Fig. 2(h)) with an adsorption energy of −3.13 eV as per eqn (2).

The formation of formic acid by the reaction of CO_2 and H occurs through a bidentate formate route. These reaction

Table 3 Binding energy (E_b) and related bond lengths of H_2, H, 2H, CO_2, HCOO and HCOOH on the Pd_2Cu_2 nanoclusters

Adsorbate species	Site	Bond lengths (Å)	E_b (eV)
H_2	Top-Pd	Pd–H = 1.75, 1.72, H–H = 0.86	−5.05
H	Top-Cu	Cu–H = 1.51	−2.05
2H	Cu–Pd bridge	Cu–H= 1.80, Pd–H = 1.75	−5.19
CO_2	Cu–Pd bridge	C–O = 1.26	−0.91
HCOO	Carboxyl	Cu–H = 2.33, Pd–O = 1.14, C–O = 1.23, 1.32, O–H = 1.03	−1.21
	Bidentate	Pd–O = 2.14, Cu–O = 1.94, C–O = 1.28, C–H = 1.11	−3.39
HCOOH	Pd–H	Pd–H = 1.96, O–H = 1.10, C–O = 1.31, C–O = 1.25, C–H = 1.10, Cu–O = 1.95	−1.37
	Cu–H	Cu–H = 2.61, O–H = 1.05, C–O = 1.32, C–O = 1.24, C–H = 1.10, Pd–O = 2.21	−1.08

2588 | *Phys. Chem. Chem. Phys.*, 2023, **25**, 2584–2594

This journal is © the Owner Societies 2023

pathways have been investigated using DFT and CI-NEB methods. The overall reaction pathway has been divided into two parts: (i) CO_2 to bidentate formation and (ii) bidentate to formic acid formation on the Pd_mCu_n ($m + n$ = 4, 8,13) clusters. The initial and final images of the reaction pathways obtained from the stable geometrics are shown in Fig. 2 and Fig. S1 and S2 (ESI†). The intermediate geometrics are obtained by NEB calculations. Formic acid formation from CO_2 on the Pd_mCu_n ($m + n$ = 4, 8, 13) clusters is discussed in the proceeding subsections.

NEB for CO_2 to formic acid conversion on Pd_2Cu_2 cluster

Based on the adsorption results, the reaction pathways for CO_2 to formic acid formation on the Pd_2Cu_2 tetramer cluster has been studied (see Fig. 3). The reaction between CO_2 and H to form formate on the Pd_2Cu_2 cluster is shown in Fig. 3(a). From the figure, it is seen that H is stable in the bridge of the Pd–Cu

(a)

(b)

Fig. 3 The potential energy profile for the formation of (a) bidentate formate by the reaction of H-atoms and CO_2 (b) formic acid by the reaction of H-atoms and formate on the Pd_2Cu_2 cluster.

edge along with a co-adsorbed CO_2 molecule. The Pd–H and Cu–H bond lengths are found to be 1.71 and 1.62 Å, respectively. This H moves from its stable site to a C-atom of CO_2 to form formate which gets attached to the Pd_2Cu_2 cluster with its two O-atoms. The intermediate images are shown in Fig. 3(a). The activation barrier for this reaction of formate formation from CO_2 is found to be 0.81 eV.

In the next NEB calculations *i.e.* the formic acid formation by the reaction of formate and a H-atom is depicted and shown in Fig. 3(b). In this graph, image 1 is the initial state where H is stable on the Pd–Pd edge of Pd_2Cu_2 along with the adsorbed bidentate formate. From the figure, it is seen that H gets transferred to the Pd–Cu edge of Pd_2Cu_2 where formate is already adsorbed with its two O-atoms, which is shown in image 3. This H is further transferred to one of the O-atoms of formate closer to the Pd atom to form formic acid as shown image 6 of Fig. 3(b). The activation barrier for this reaction of formate and H to formic acid is found to be 0.79 eV which is more or less similar to the previous step of formate formation.

CO_2 hydrogenation to formic acid on Pd_4Cu_4 octamer

In line with the study for CO_2 hydrogenation on the Pd_2Cu_2 cluster, we have started investigating the adsorption behaviour of H_2 on the Pd_4Cu_4 cluster. The optimization has been performed by placing the H_2 molecule in on-top positions of the Pd and Cu sites along with the other bridge and hollow sites available on the cluster. The distance of the Pd/Cu to H is kept at ~ 3 Å. The results suggest that H_2 favours the on-top Cu site (Fig. S1(a), ESI†) with an adsorption energy of -4.91 eV. The two Cu–H bond distances are 1.68 Å and the H–H bond is elongated up to 0.83 Å. The adsorption of the H-atom on the top, bridge and hollow sites of the Pd_4Cu_4 cluster is also investigated. Among different configurations, the H atoms prefer the hollow site of a triangle formed by two Pd and one Cu atom (Fig. S1(b), ESI†). The adsorption energy for this is -2.87 eV with an average Pd–H distance of 1.75 Å. The stability of two H atoms on the Pd_4Cu_4 cluster has also been investigated. It is found that both of the H atoms prefer to bind with the Cu–Pd and Pd–Pd bridge sites as shown in (Fig. S1(c), ESI†). The binding energy for these two H atoms is calculated to be -5.87 eV with Cu–H and Pd–H bond lengths of 1.76 and 1.82 Å, respectively.

Like Pd_2Cu_2, CO_2 adsorption on this Pd_4Cu_4 cluster is also studied by placing the molecule at different well-defined sites. It is found that the CO_2 molecule gets adsorbed in a V-shaped fashion on the Pd_4Cu_4 cluster as shown in Fig. S1(d) (ESI†). The adsorption energy for this configuration is -0.96 eV. The Cu–O and Pd–C bonds are 1.93 and 1.98 Å, respectively. One of the C–O bonds attached to Cu–Pd edge of the Pd_4Cu_4 octamer is elongated from 1.16 to 1.26 Å. The adsorption nature of the CO_2 molecule in the Pd_4Cu_4 cluster is same as that on the Pd_2Cu_2 moiety and the reason lies within the nature of bonding. Like Pd_2Cu_2, here formic acid formation on the Pd_4Cu_4 cluster takes place through the formate route. The HCOO species can be adsorbed in two forms, carboxyl (mono HOCO) and bidentate (bi-HCOO) depending on the number of oxygen atoms that get
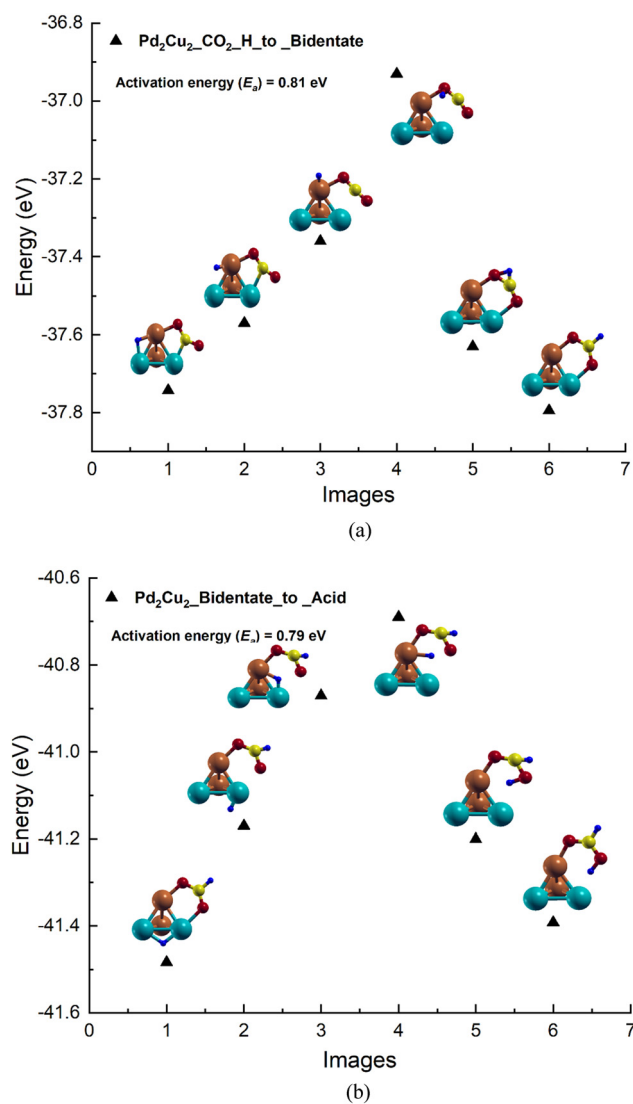
attached to the Pd$_4$Cu$_4$ cluster. In case of carboxyl binding, O and C-atoms are attached to Pd and C atoms, respectively as shown in Fig. S1(f) (ESI†). The Pd–O and Cu–C bond distances are 1.99 Å each and the adsorption energy for monodentate carboxyl HOCO is −2.44 eV.

Like, for the Pd$_2$Cu$_2$ cluster, the co-adsorption of H and CO$_2$ has been compared with H and HCOO on the Pd$_4$Cu$_4$ cluster.

In the case of bidentate HCOO, it binds to the Pd–Cu edge of the Pd$_4$Cu$_4$ cluster where Cu is in the octahedron frame and Pd atom is out of the frame (Pd–Pd edge) as shown in Fig. S1(g) (ESI†). The Pd–O and Cu–O bond distances are 2.09 and 1.91 Å, respectively. The adsorption energy is found to be −3.67 eV. The C–H bond distance and O–C–O bond angle are 1.11 Å and 104°, respectively. It is interesting to report that CO$_2$ gets adsorbed to a Cu–Pd edge of Pd$_4$Cu$_4$ through a C bond and in a V-shape fashion (Fig. S1(d), ESI†) but addition of a H atom to a C-atom in CO$_2$, resulting in bidentate formate HCOO, favors the inverted V-shaped form for the adsorption of bidentate formate (bi-HCOO). The reason is depicted in the electronic structure analysis in the Electronic structure section.

The final step is formic acid formation from bidentate formate by addition of an H-atom. Adsorption of formic acid on the Pd$_4$Cu$_4$ cluster has two possibilities; the H atom is either attached to a Cu or a Pd atom of the cluster. It has been found that the protonic H atom of the HCOOH is attached to the Pd atom of the Pd$_4$Cu$_4$ with an adsorption energy of −1.17 eV (Fig. S1(i), ESI†). However, the adsorption of H with Cu is not stable. The adsorption energy of this adsorbed formic acid configuration is −1.37 eV. The Pd–H and Cu–O distances of this adsorbed formic acid configuration are 1.94 Å and 1.93 Å, respectively.

Like, Pd$_2$Cu$_2$, the co-adsorption of H atoms and CO$_2$ as well as H atoms and formate HCOO have been studied on the Pd$_4$Cu$_4$ cluster. Among different isomeric geometries, the H atom favors the hollow site (a triangle composed of two Pd and Cu atoms) as shown in Fig. S1(e) (ESI†). The position of the CO$_2$ is fixed and it is attached to the Pd–Cu edge adjacent to the H atom adsorption site. The H-adsorption energy for this Pd$_2$Cu$_2$–CO$_2$ moiety is found to be −2.60 eV as per equation (2). Similarly, a H atom in the same position *i.e.* in the mid of the triangle composed of two Pd and Cu atoms, adjacent to the adsorbed bidentate formate site, has the lowest energy structure as shown in Fig. S1(h) (ESI†). The H-adsorption energy for this Pd$_2$Cu$_2$–HCOO moiety is found to be −2.79 eV. The binding energies and related bond lengths of H$_2$, H, 2H, CO$_2$, HCOO and HCOOH adsorbed on the Pd$_4$Cu$_4$ nanocluster are given in Table S1 (ESI†).

NEB for CO$_2$ to formic acid conversion on Pd$_4$Cu$_4$ cluster

After investigating the formic acid formation on the Pd$_2$Cu$_2$ cluster, we have studied the same process on the higher order cluster Pd$_4$Cu$_4$. Here also, the process of formic acid formation has been divided into two parts *i.e.* CO$_2$ to formate and formate to formic acid formation. Fig. S3(a) (ESI†) shows the bidentate formate formation pathway by the reaction of CO$_2$ and H-atoms on a dodecahedron Pd$_4$Cu$_4$ cluster. The initial image of this

NEB calculation is that H is stable on the Pd–Cu edge with CO$_2$ adsorbed on the adjacent Pd–Cu edge. The overall reaction pathway as shown in Fig. S3(a) (ESI†) shows the H atom movement from its stable position to the C atom of CO$_2$ to form formate. The activation barrier for this reaction is found to be 0.79 eV.

In the next step, the reaction pathway for formate to formic acid formation on the Pd$_4$Cu$_4$ octahedron is shown in Fig. S3(b) (ESI†). Here the H-atom on the Pd–Cu edge of Pd$_4$Cu$_4$ has a stable position along with the formate adsorbed on the adjacent Pd–Cu edge. The NEB calculation shows the H movement from its stable position to the O-atom which was attached to the Pd atom in the formate. The activation energy for this reaction is calculated to be 0.68 eV which is lower compared to the first step of formate formation on this Pd$_4$Cu$_4$ cluster.

CO$_2$ hydrogenation to formic acid on Pd$_{12}$Cu cluster

At first, the adsorption properties of H$_2$ molecules on the Pd$_{12}$Cu icosahedron cluster have been studied. For that, a H$_2$ molecule was placed on the top of the Pd atom at a distance of ~3 Å, setting the H–H bond length equal to the value of the free H$_2$ molecule, 0.75 Å. The H$_2$ at the top of the Pd-atom has the lowest energy structure as shown in Fig. S2(a) (ESI†). The adsorption energy of the H$_2$ molecule adsorbed on this top Pd atom is found to be −5.06 eV. The two Pd–H bond distances are optimized to 1.70 Å, whereas the H–H bond distance is 0.88 Å.

Now the adsorption of the H-atom on different sites (top, bridge and hollow) of the Pd$_{12}$Cu icosahedron cluster is also investigated. Among the different structures, it has been found that the H at the mid of the triangle constituted by three Pd atoms has the stable structure as shown in Fig. S2(b) (ESI†). The adsorption energy and average Pd–H distance are −2.85 eV and 1.83 Å, respectively. The stability of two H atoms on the Pd$_{12}$Cu cluster has also been investigated. It is found that both the H atoms prefer to bind with the three Pd atom hollow sites (fcc and hcp) as shown in (Fig. S2(c), ESI†). The binding energy for these two H atoms is calculated to be −5.13 eV with an average Pd–H bond length of 1.83 Å, respectively.

After studying the adsorption of H$_2$ molecules and H-atoms, the adsorption of CO$_2$ gas molecules on the Pd$_{12}$Cu icosahedron cluster and the energetics associated with that have been investigated. It has been observed that one C–O bond, of bond length 1.27 Å, of the CO$_2$ molecules is parallelly attached to the Pd–Pd bond of the CuPd$_{12}$ cluster as shows in Fig. S2(d) (ESI†). The other O-atom of that CO$_2$ molecule is not bonded to any atom of that cluster. Initially a linear CO$_2$ molecule is placed parallelly to the Pd–Pd edge of the Pd$_{12}$Cu cluster. In the most stable geometry the shape of the CO$_2$ molecule became V-shaped with an O–C–O bond angle of 105°. The adsorption geometry together with the calculated binding energy of −0.44 eV implies that the CO$_2$ molecule is bonded to the cluster.

Both by experiment and theoretical studies, it is established that HCOO is a key intermediate for CO$_2$ hydrogenation to formic acid and methanol.[45,46] There are two configurations of

2590 | *Phys. Chem. Chem. Phys.*, 2023, **25**, 2584–2594

This journal is © the Owner Societies 2023

HCOO species, carboxyl (mono-HOCO) and bidentate (bi-HCOO), distinguished by the number of O atoms that are adsorbed on the $Pd_{12}Cu$ cluster. For carboxyl (mono-HOCO), the C–O bond of HOCO binds to the Pd–Pd edge of the $Pd_{12}Cu$ cluster as shown in Fig. S2(f) (ESI†). The O–H bond of HOCO does not attach to the cluster, it remains attached to the C-atom. The Pd–C, Pd–O and C–O bond lengths of mono-HOCO adsorbed on the $Pd_{12}Cu$ cluster are found to be 1.96, 2.26 and 1.25 Å, respectively. The adsorption energy for this mono-HOCO moiety is −2.50 eV. For, bidentate-HCOO, it binds to the Pd–Pd edge of the $Pd_{12}Cu$ cluster through two O-atoms (see Fig. S2(g), ESI†) with an adsorption energy of −3.22 eV. The two Pd–O bond lengths are identical at 2.10 Å.

The co-adsorptions of H atoms and CO_2 as well as H atoms and formate HCOO on the icosahedron $Pd_{12}Cu$ cluster are similar to those on the Pd_mCu_n ($m + n = 4, 8$) clusters. Among the different isomeric geometries, the H atom is found to be most stable in the mid of the triangle composed of three Pd atoms as shown in Fig. S2(b) (ESI†). The position of the CO_2 is fixed and it is attached to the Pd–Pd edge adjacent to the H atom adsorption site (Fig. S2(e), ESI†). The H-adsorption energy for this $Pd_{12}Cu$-CO_2 moiety is found to be −2.87 eV. Similarly, the H atom in the same position *i.e.* in the mid of the triangle composed of three Pd atoms, adjacent to the adsorbed bidentate formate site, has the lowest energy structure as shown in Fig. S2(h) (ESI†). The H-adsorption energy for this $Pd_{12}Cu$–HCOO moiety is found to be −2.84 eV.

After formate adsorption, we turned our attention to adding an H atom to formate to produce a formic acid molecule on the $Pd_{12}Cu$ cluster. For the adsorption of the final product formic acid on the $Pd_{12}Cu$ cluster, there are two possibilities of HCOOH adsorption, where the two H-atoms are in *cis* and *trans* positions. The *trans* configuration (shown in Fig. S2(i), ESI†) is found to be 0.43 eV more stable than the cis one. The Pd–H and Pd–O bond distances in the *trans* configuration are 2.16 and 2.19 Å, respectively. The adsorption energy for that *trans* species is −0.90 eV. The binding energies and related bond lengths of H_2, H, 2H, CO_2, HCOO and HCOOH adsorbed on the $Pd_{12}Cu$ nanocluster are given in Table S2 (ESI†).

NEB for CO_2 to formic acid conversion on $Pd_{12}Cu$ cluster

In this case, the process of formic acid formation from CO_2 has also been divided into two parts like the previous two clusters (i) CO_2 to bidentate formate (ii) formate to formic acid. The first step is the reaction of CO_2 and H to form bidentate formate, which is shown in Fig. S4(a) (ESI†). Here, all of the adsorbed species *i.e.* CO_2 and H-atoms are on the Pd–Pd edge as the outer shell of the $Pd_{12}Cu$ cluster is made up with Pd atoms. The H-atom moves from the Pd–Pd edge to the adjacent CO_2. At first, it goes to one of the O-atoms of CO_2 and is then transferred to the C atom of that CO_2 to form formate. The activation barrier for the reaction is found to be 1.92 eV which is higher than the same process on the Pd_2Cu_2 and Pd_4Cu_4 clusters.
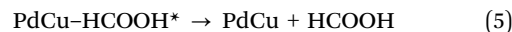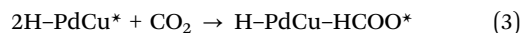
For the bidentate formate to formic acid conversion the H-atom moves from the Pd–Pd edge to the apex Pd-atom with

which one of the O-atoms of formate (HCOO) is attached as shown in image 3 of Fig. S4(b) (ESI†). This H-atom further gets attached to that O-atom and forms formic acid where two H-atoms are in the *trans* position with respect to each other. The activation barrier for the reaction is found to be 1.77 eV.

From the six NEB calculations (Fig. 3 and Fig. S3, S4, ESI†), it is seen that, formate and formic acid formation require more energy in the $Pd_{12}Cu$ cluster compare to that in the Pd_mCu_n ($m + n = 4, 8$) clusters. The reason may be the Pd–Cu and Pd–Pd edge of the clusters where CO_2 and formate HCOO got adsorbed. Also, the activation energy for CO_2 to formate and formate to formic acid formation decreases as the PdCu cluster size increases except for the stable $Pd_{12}Cu$ magic cluster.

Thermochemistry of CO_2 hydrogenation to formic acid

Depending on the stability of the H_2 molecule and the two H atoms on the Pd_mCu_n ($m + n = 4, 8$ and 13) clusters, we have extended our study to the hydrogenation of CO_2 to formic acid *via* the formate route on these clusters. The overall reaction can be given as follows:

$$H_2 + PdCu \rightarrow H_2\text{–}PdCu^* \qquad (1)$$

$$H_2\text{–}PdCu^* \rightarrow 2H\text{–}PdCu^* \qquad (2)$$

$$2H\text{–}PdCu^* + CO_2 \rightarrow H\text{–}PdCu\text{–}HCOO^* \qquad (3)$$

$$H\text{–}PdCu\text{–}HCOO^* \rightarrow PdCu\text{–}HCOOH^* \qquad (4)$$

$$PdCu\text{–}HCOOH^* \rightarrow PdCu + HCOOH \qquad (5)$$

Here the PdCu = Pd_mCu_n ($m + n = 4, 8$ and 13) clusters and the (*) mark denotes the species in their adsorbed state. The reaction energies of each elementary reaction have been calculated. The potential energy diagram for the hydrogenation of CO_2 on the Pd_mCu_n ($m + n = 4, 8$ and 13) clusters is shown in Fig. 4. The most stable adsorption configurations of these clusters have been chosen as the initial states. In the first step
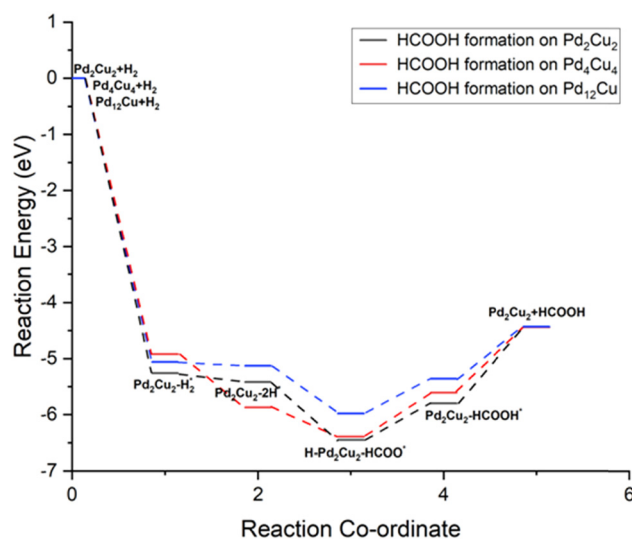

Fig. 4 Potential energy diagram of CO_2 hydrogenation to formic acid on the Pd_mCu_n ($m + n = 4, 8$ and 13) clusters.

This journal is © the Owner Societies 2023

Phys. Chem. Chem. Phys., 2023, **25**, 2584–2594 | **2591**

(reaction (1)), a H_2 molecule gets adsorbed firstly at the top site with the formation of either Pd–H (for Pd_2Cu_2 and $Pd_{12}Cu$) or Cu–H (Pd_4Cu_4) bonds. The reaction energies for this adsorption reaction are found to be −5.05, −4.91, −5.06 eV for the Pd_2Cu_2, Pd_4Cu_4 and $Pd_{12}Cu$ clusters, respectively. In the second step (reaction (2)), the adsorbed H_2 molecule gets dissociated into two H atoms. These two H atoms are found to be stable at the three atom hollow site or bridge site for these three clusters as shown in Fig. 1. This reaction is found to be exothermic and the reaction energies are calculated to be −0.17, −0.95 and −0.07 eV for the Pd_2Cu_2, Pd_4Cu_4 and $Pd_{12}Cu$ clusters, respectively. In the third step (reaction (3)), which is one of the most important steps, CO_2 interacts with the 2H–PdCu species and forms formate as the stable adsorbed group with one H atom located at the nearby bridge or three atom hollow sites. The reaction is also found to be exothermic with reaction energies of −1.02, −0.52 and −0.84 eV for the Pd_2Cu_2, Pd_4Cu_4 and $Pd_{12}Cu$ clusters, respectively. In the next step (reaction (4)), the H atom, located at a nearby site, diffuses to the formate group and forms formic acid which remains adsorbed to the cluster with its O atom centre. This reaction is found to be endothermic for all of the clusters under study. The reaction energy for this reaction on the Pd_2Cu_2, Pd_4Cu_4 and $Pd_{12}Cu$ clusters are found to be 0.65, 0.79 and 0.62 eV, respectively. The final step of the process (reaction (5)) is desorption of the formic acid molecule from the cluster. The reaction is also found to be endothermic with reaction energies of 1.37, 1.17 and 0.92 eV for the Pd_2Cu_2, Pd_4Cu_4 and $Pd_{12}Cu$ clusters, respectively. For all of the clusters, as the reaction energy for this last step is higher compared to the other steps, it is regarded as the rate determining step of the overall process of hydrogenation of CO_2 to formic acid. The enthalpies for the overall process on the Pd_2Cu_2, Pd_4Cu_4 and $Pd_{12}Cu$ clusters are found to be 0.83, 0.48 and 0.63 eV, respectively.

Electronic structure

Adsorption of CO_2 on the Pd_mCu_n ($m + n = 4$, 8 and 12) clusters is the crucial step for the formation of formic acid and methanol either through the formate or carboxyl route. The reason behind the adsorption of CO_2 on these clusters in a particular fashion needs to be explored. From the Fig. 2(d) and Fig. S1(d) and S2(d) (ESI†), it is seen that CO_2 gets adsorbed either on the Pd–Cu edge (for Pd_2Cu_2 and Pd_4Cu_4 clusters) or on the Pd–Pd edge of the $Pd_{12}Cu$ icosahedron cluster. In the Pd_mCu_n ($m + n = 4$, 8 and 12) clusters, a linear CO_2 molecule has been placed in various positions like on top of Pd, on top of Cu, on the Pd–Pd edge, on the Cu–Cu edge, at the mid of the Pd–Cu–Cu triangle, at the mid of the Pd–Pd–Cu triangle *etc.* Among those, CO_2 gets adsorbed on the Pd–Cu edge in an inverted V-shaped fashion with the C-centre attached to the Pd-atom and one O-centre attached to the Cu atom of the clusters. The other O-atom of the CO_2 remains unattached to any Pd or Cu atom of these clusters. A similar configuration for CO_2 adsorption has been seen in the case of the Pd_4Cu_4 and $Pd_{12}Cu$ clusters also.

To understand the nature of the chemical bonding present in the CO_2 adsorbed Pd_2Cu_2 cluster, the total and orbital projected density of states for Pd_2Cu_2 and Pd_2Cu_2–CO_2 have been calculated and shown in Fig. S5 and S6 (ESI†). From the Fig. S5(b) (ESI†), it is seen that the Pd-4d and Cu-3d orbitals are mainly contributing to the Fermi energy in the Pd_2Cu_2 cluster, whereas in the Pd_2Cu_2–CO_2 moiety, the 2p orbital of the C and O atoms are contributing along with the Pd-4d and Cu-3d orbitals (Fig. S6(b), ESI†). The presence of finite DOS at the Fermi level indicates the metallic nature and the electron conduction behaviour of the Pd_2Cu_2 and Pd_2Cu_2–CO_2clusters. In Fig. S6(b) (ESI†), the DOS peaks of the C-atom which range from 0–5 eV are overlapping with DOS of the Pd atom to which it is attached. Whereas, the DOS spectra of one of the O-atoms (^{1}O atom) of the CO_2 is overlapping with those of Cu atom to which it is attached. The DOS spectra (p-orbital DOS) of the other O-atom (^{2}O atom) which is not attached to any Pd or Cu atoms has its position much below the Fermi level mainly ranging from −12.5 eV to −5 eV. From the charge density distribution table given in Table S6 (ESI†), it is seen that the C-atom takes charges from two O-atoms and donates that to one Pd atom of the Pd–Cu edge of the Pd_2Cu_2 cluster. Whereas, the Cu atom of that Pd–Cu edge donates charges to one of the O-atoms of the CO_2 (^{1}O atom) to which it is attached and becomes an electron deficient centre. This charge transfer facilitates the bond formation between the Pd–Cu edge and the CO_2 molecule and helps the CO_2 molecule to get adsorbed on that edge in an inverted V-shaped fashion. A similar type of bonding and charge transfer has been seen in the case of the Pd_4Cu_4 cluster and its CO_2 adsorbed counterpart. The supporting information of the charge density distribution is given in Table S7 (ESI†).

After exploring the nature of the bonding in the Pd_2Cu_2 and Pd_4Cu_4 clusters and their CO_2 adsorbed counter parts, the same has been investigated for the $Pd_{12}Cu$ clusters and its CO_2 adsorbed species in terms charge density distributions. From the charge density distribution table given in Table S8 (ESI†), it is seen that one of the two Pd atoms of the Pd–Pd edge (^{1}Pd atom) to which the C atom of CO_2 is attached acts as an electron depletion centre as it receives electronic charges from two O atoms *via* a C-atom centre. Another Pd atom of that Pd–Pd edge (^{2}Pd atom) donates electronic charges to the O-atom of the CO_2 to which it is attached and it becomes an electron deficient centre. This promotes the CO_2 to get adsorbed in an inverted V-shaped way like the previous cases for the Pd_2Cu_2 and Pd_4Cu_4 clusters.

Computational details

All calculations are performed within the spin-polarized density functional theory using the plane wave-pseudopotential approach as implemented in the Vienna *ab initio* simulation package (VASP).[47–49] The electron-ion interaction and the exchange correlation energy are described under the projector-augmented wave (PAW) method and the generalized gradient

2592 | *Phys. Chem. Chem. Phys.*, 2023, **25**, 2584–2594

This journal is © the Owner Societies 2023

approximation (GGA) of Perdew–Burke–Ernzerhof (PBE), respectively.[50–52] The energy cut off for the plane wave basis set has been fixed at 500 eV for assuming a good energy convergence. Finding the ground state structure of a cluster is a challenging task. For this, several methods like, Generic Algorithm, basin-hoppins, evolutionary algorithm are used to generate a large number of geometries. However, for small clusters one can use chemical intuition, which in other words is called an educated guess structure and one can then relax these structures to the possible nearest minima. Following this, we have generated a large number of initial geometries and found out the lowest energy structure for each composition.[53–55] A large number of spin states have also been considered for all these structures. The ionic optimization has been carried out using the conjugate gradient scheme and the forces on each ion are minimized up to 5 meV Å^{-1}.[56,57] A suitable simulation box of size $15 \times 15 \times 15$ Å has been considered for all of the calculations. The k-point sampling in the Brillouin zone (BZ) are treated with the Monkhorst–Pack scheme, using the gamma point.[58] The total energies of each relaxed structure using the linear tetrahedron method with Blochl corrections have been subsequently calculated in order to eliminate any broadening-related uncertainty in the energies.[59] In all of the DFT based calculations, the electrons are described by the scalar-relativistic approximation, in which spin–orbit coupling (SOC) is taken into account for the core states but is neglected for the valence states.[60,61] However, few studies have showed that SOC plays a crucial role for heavy element systems.[62–64] Due to the presence of Pd atoms, here in this work, DFT-PBE calculations with and without SOC for the valence states have been performed for the dimers. The binding energies (E_b) of the Pd_mCu_n ($m + n = 2, 4, 8,$ and 13) clusters have been estimated from the total energy calculations using eqn (6)

$$E_b(Pd_mCu_n) = \frac{\{E_{Pd_mCu_n} - m \cdot E_{Pd\text{-atom}} - n \cdot E_{Cu\text{-atom}}\}}{(m+n)} \quad (6)$$

where, $E_{Pd_mCu_n}$ = total energy of the Pd_mCu_n cluster, $E_{Pd\text{-atom}}$ = total energy of the Pd atom, $E_{cu\text{-atom}}$ = total energy of the Cu atom, m = total number of the Pd atom(s) and n = total number of the Cu atom(s).

The adsorption energies of adsorbate on the Pd_mCu_n ($m + n = 4, 8$ and 13) clusters, E_{ads} have been calculated by eqn (7)

$$E_{ads} = E_{adsorbate+cluster} - (E_{adsorbate} + E_{cluster}) \quad (7)$$

$E_{adsorbate+cluster}$ = total energy of the adsorbate and cluster, $E_{adsorbate}$ = total energy of the adsorbate and $E_{cluster}$ = total energy of the cluster.

Conclusion

In summary, CO_2 adsorption and hydrogenation on Pd_mCu_n ($m + n = 4, 8$ and 13) clusters have been studied using DFT calculations. The stable adsorbed structures of the possible intermediates like adsorbed H_2 molecules, one H atom, two H atoms, CO_2 molecule, CO_2 molecules with one H atom *etc.* have been evaluated and the energetics associated with those have

been calculated. It has been found that CO_2 got adsorbed on these clusters in an inverted V-shaped fashion and CO_2 hydrogenation occurs through a formate intermediate. The first hydrogenation to formate goes through a unidentate structure which later transforms to a more stable bidentate structure easily. The second hydrogenation from formate to formic acid is energetically less difficult. An investigation of the possible pathways of forming formic acid on Pd_mCu_n ($m + n = 4, 8$ and 13) clusters is reported. The reaction energies for the CO_2 hydrogenation to formic acid on all of the clusters have also been calculated. The nature of chemical bonding present between the adsorbate and adsorbent was investigated by electronic structure analysis. The calculated results provide a potential candidate for formic acid synthesis and the present study can be useful for CO_2 conversion and utilization with Pd–Cu bimetallic catalysts.

Data availability

The data that support the findings of this study are available on request from the corresponding author. The data are not publicly available due to ethical restrictions.

Conflicts of interest

There are no conflicts to declare.

Acknowledgements

References

1 C. Song, *Catal. Today*, 2006, **115**, 2–32.
2 Y. Yang, M. G. White and P. Liu, *J. Phys. Chem. C*, 2011, **116**, 248–256.
3 Y. F. Zhao, Y. Yang, C. Mims, C. H. F. Peden, J. Li and D. Mei, *J. Catal.*, 2011, **281**, 199–211.
4 Y. Yang, J. Evans, J. A. Rodriguez, M. G. White and P. Liu, *Phys. Chem. Chem. Phys.*, 2010, **12**, 9909–9917.
5 W. Leitner, *Angew. Chem., Int. Ed. Engl.*, 1995, **34**, 2207–2221.
6 P. G. Jessop, T. Ikariya and R. Noyori, *Chem. Rev.*, 1995, **95**, 259–272.
7 M. Zhang, M. Dou and Y. Yu, *Appl. Surf. Sci.*, 2019, **433**, 780–789.
8 J. Yoshihara, S. Parker, A. Schafer and C. T. Campbell, *Catal. Lett.*, 1995, **31**, 313–324.
9 M. D. Porosoff and J. G. Chen, *J. Catal.*, 2013, **301**, 30–37.

This journal is © the Owner Societies 2023

Phys. Chem. Chem. Phys., 2023, **25**, 2584–2594 | **2593**

10 L. Liu, H. Yao, Z. Jiang and T. Fang, *Appl. Surf. Sci.*, 2018, **451**, 333–345.

11 G. Centi and S. Perathoner, *Catal. Today*, 2009, **148**, 191–205.

12 Y. Tan, W. Nookuea and H. Li, *Energy Covers Manage*, 2016, **118**, 204–222.

13 M. P. Fortes, A. B. Dumitriu and E. T. Zimas, *Energy Procedia*, 2014, **63**, 7968–7975.

14 S. T. Yong, C. W. Ooi, S. P. Chai and X. S. Wu, *Int. J. Hydrogen Energy*, 2013, **38**, 9541–9552.

15 M. P. Fortes, J. C. Schoneberger, A. Boulamanti, G. Harrison and E. Tzimas, *Int. J. Hydrogen Energy*, 2016, **41**(37), 16444–16462.

16 A. Alvarez, A. Bansode, A. Urakawa, A. V. Bavykina, T. A. Wezendonk, M. Makkee, J. Gascon and F. Kapteijn, *Chem. Rev.*, 2017, **117**, 9804–9838.

17 J. Klankermayer and W. Leitner, *Philos. Trans. R. Soc., A*, 2016, **374**, 20150315.

18 X. Jiang, Y. Jiao, C. Moran, X. Nie, Y. Gong, X. Guo, K. S. Walton and C. Song, *Catal. Commun.*, 2019, **118**, 10–14.

19 L. Liu, F. Fan, M. Bai, F. Xue, X. Ma, Z. Jiang and T. Fang, *Mol. Catal.*, 2019, **466**, 26–36.

20 Y. Yang, M. G. White and P. Liu, *J. Chem. C*, 2012, **116**, 248–256.

21 C. L. Chiang, K. S. Lin, H. W. Chuang and C. M. Wu, *Int. J. Hydrogen Energy*, 2017, **42**, 23647–23663.

22 I. Melian-Cabrera, M. L. Granados and J. L. G. Fierro, *Catal. Lett.*, 2002, **79**, 165–169.

23 D. Heyl, U. Rodemerck and U. Bentrup, *ACS Catal.*, 2016, **6**, 6275–6284.

24 W. Wang, S. Wang, X. Ma and J. Gong, *Chem. Soc. Rev.*, 2011, **40**, 3703–3727.

25 C. Hao, S. Wang, M. Li, L. Kang and X. Ma, *Catal. Today*, 2011, **160**, 184–190.

26 D. N. Sredojevic, Z. Sljivancanin, E. N. Brothers and M. R. Belic, *ChemistrySelect*, 2018, **3**, 2631–2637.

27 G. Peng, S. J. Sibener, G. C. Schatz, S. T. Ceyer and M. Mavrikakis, *J. Phy Chem C*, 2012, **116**, 3001–3006.

28 L. Gong, J. J. Chen and Y. Mu, *Phys. Chem. Chem. Phys.*, 2017, **19**, 28344–28353.

29 G. Liu, P. Poths, X. Zhang, Z. Zhu, M. Marshall, M. Blankenhorn, A. N. Alexandrova and K. H. Bowen, *J. Am. Chem. Soc.*, 2020, **142**, 7930–7936.

30 N. Kumar, D. Chattaraj, P. Ghosh and C. Majumder, *J. Phys. Chem. C*, 2018, **122**, 12920–12933.

31 I. Shim and K. Gingerich, *J. Chem. Phys.*, 1984, **80**, 5107–5119.

32 K. Huber and G. Herzberg, *Molecular Spectra and Molecular Structure. IV. Constants of Diatomic Molecules*, Van Nostrand Reinhold Company, New York, 1979.

33 M. Mors, *Advances in Metal and Semiconductor Clusters*, JAI Press, Greenwich, CT, 1993.

34 R. Ram, C. Jarman and P. Bernath, *J. Mol. Spectrosc.*, 1992, **156**, 468–486.

35 H. Kahnouji, H. Najafvandzadeh, S. Javad Hashemifar, M. Alaei and H. Akbarzadeh, *Chem. Phys. Lett.*, 2015, **630**, 101–105.

36 Y. Du, H. Sheng, D. Astruc and M. Zhu, *Chem. Rev.*, 2020, **120**, 526–622.

37 A. Mravak, S. Vajda and V. Bonacic-Kuutecky, *J. Phys. C.*, 2022, **126**, 18306–18312.

38 C. Goswami, H. Saikia, B. J. Borah, M. J. Kalita, K. Tada, S. Tanaka and P. Bharali, *J. Colloid Interface Sci.*, 2021, **587**, 446–456.

39 H. Koga, A. Hayashi, Y. Ato, K. Tada, S. Tanaka and M. Okumura, *Catal. Today*, 2019, **331**, 236–244.

40 S. Maheswari, S. Karthikeyanm, P. Murugan, P. Sridhar and S. Pitchumani, *Phys. Chem. Chem. Phys.*, 2012, **14**, 9683–9695.

41 H. Li, L. Li, A. Pederson, Y. Gao, N. Khetrapal, H. Jónsson and X. C. Zeng, *Nano Lett.*, 2015, **15**, 682–688.

42 R. Pal, A. Poddar and P. K. Chattaraj, *Front. Chem.*, 2021, **9**, 730548.

43 R. Varns and P. Strange, *Phys. Status Solidi B*, 2012, **249**(11), 2179–2189.

44 Y. Rao, Y. Lei, X. Cui, Z. Lin and F. Chen, *J. Alloys Compd.*, 2013, **563**, 50–55.

45 Y. Li, S. H. Chan and Q. Sun, *Nanoscale*, 2015, **7**, 8663–8683.

46 S. Kattel, P. J. Ramirez, J. G. Chen, J. Rodriguez and P. Liu, *Science*, 2017, **355**, 1296–1299.

47 G. Kresse and J. Hafner, *Phys. Rev. B: Condens. Matter Mater. Phys.*, 1994, **49**, 14251–14269.

48 G. Kresse and J. Furthmüller, *Comput. Mater. Sci.*, 1996, **6**, 15–50.

49 W. Kohn and L. Sham, *Phys. Rev. A*, 1965, **140**, 1133–1138.

50 P. E. Blöchl, *Phys. Rev. B: Condens. Matter Mater. Phys.*, 1994, **50**, 17953–17979.

51 G. Kresse and D. Joubert, *Phys. Rev. B: Condens. Matter Mater. Phys.*, 1999, **59**, 1758–1775.

52 J. P. Perdew, K. Burke and M. Ernzerhof, *Phys. Rev. Lett.*, 1996, **77**, 3865–3868.

53 V. Blum, R. Gehrke, F. Hanke, P. Havu, V. Havu, X. Ren, K. Reuter and M. Scheffler, *Comput. Phys. Commun.*, 2009, **180**, 2175–2196.

54 S. Bhattacharya, S. Levchenko, L. Ghiringhelli and M. Scheffler, *Phys. Rev. Lett.*, 2013, **111**(135501), 1–5.

55 S. Bhattacharya, S. Levchenko, L. Ghiringhelli and M. Scheffler, *New J. Phys.*, 2014, **16**, 123016 (1–34).

56 R. P. Feynman, *Phys. Rev.*, 1939, **56**, 340–343.

57 H. Hellman, *Introduction to Quantum Chemistry*, Deuticke, Leipzig, 1937.

58 H. J. Monkhorst and J. D. Pack, *Phys. Rev. B: Condens. Matter Mater. Phys.*, 1976, **13**, 5188–5192.

59 P. E. Blöchl, O. Jepsen and O. K. Andersen, *Phys. Rev. B: Condens. Matter Mater. Phys.*, 1994, **49**, 16223–16233.

60 D. D. Koelling and B. N. Harmon, *J. Phys. C: Solid State Phys.*, 1977, **10**, 3107–3114.

61 T. Takeda, *Z. Phys. B: Condens. Matter Quanta*, 1978, **32**, 43–48.

62 M. J. Piotrowski, P. Piquini and J. L. F. Da Silva, *Phys. Rev. B: Condens. Matter Mater. Phys.*, 2010, **81**, 155446.

63 O. D. Häberlen, S.-C. Chung, M. Stener and N. Rösch, *J. Chem. Phys.*, 1997, **106**, 5189–5201.

64 M. N. Huda, M. K. Niranjan, B. R. Sahu and L. Kleinman, *Phys. Rev. A: At., Mol., Opt. Phys.*, 2006, **73**, 053201.